JACS
JOURNAL OF THE AMERICAN CHEMICAL SOCIETY

Communication

pubs.acs.org/JACS

Handedness Enantioselection of Carbon Nanotubes Using Helical Assemblies of Flavin Mononucleotide

Sang-Yong Ju,[‡,§,⊥] Darlington C. Abanulo,[‡,⊥] Christopher A. Badalucco,[†] José A. Gascón,[†] and Fotios Papadimitrakopoulos*[,‡,†]

[†]Nanomaterials Optoelectronics Laboratory (NOEL), Polymer Program, Institute of Materials Science and [‡]Department of Chemistry, University of Connecticut, Storrs, Connecticut 06269-3136, United States

Supporting Information

ABSTRACT: In order to truly unlock advanced applications of single-walled carbon nanotubes (SWNTs), one needs to separate them according to both chirality and handedness. Here we show that the chiral D-ribityl phosphate chain of flavin mononucleotide (FMN) induces a right-handed helix that enriches the left-handed SWNTs for all suspended (*n*,*m*) species. Such enantioselectivity stems from the sp^3 hybridization of the N atom anchoring the sugar moiety to the flavin ring. This produces two FMN conformations (*syn* and *anti*) analogous to DNA. Electrostatic interactions between the neighboring uracil moiety and the 2′-OH group of the side chain provide greater stability to the *anti*-FMN conformation that leads to a right-handed FMN helix. The right-handed twist that the FMN helix imposes to the underlying nanotube, similar to "Indian burn", causes diameter dilation of only the left-handed SWNTs, whose improved intermolecular interactions with the overlaying FMN helix, impart enantioselection.

Molecular recognition constitutes a central scheme for enantiomeric selection in self-assembly.[1] The atomically smooth graphene surface of single-walled carbon nanotubes (SWNTs), is identified by a pair of (*n*,*m*) indices that defines their chirality.[2] Apart from zigzag (*n*,0) and armchair (*n*,*n*)-SWNTs, all remaining nanotube species are composed of two enantiomers, (*n*,*m*) and (*m*,*n*). By convention, when *n* is greater than *m*, the species is right-handed or *P* for positive, and when *m* is greater than *n*, the species is left-handed or *M* for negative.[3] Unfortunately, current synthetic methods produce multiple (*n*,*m*)-SWNTs chiralities with both left- and right-handed species. As a result of this, numerous separation methodologies have been devised to enrich SWNTs according to chirality[4,5] and handedness.[3a,4b,e,6] Handedness enrichment was first introduced by the pioneering work of Komatsu et al.[3a] via chiral diporphyrin tweezers that show a preferential adsorption toward one of the two SWNT enantiomers. Subsequent work has optimized these tweezers to fine-tune their diameter selectivity as well.[6] In a diametrically opposed approach, Hersam's group realized that the chirality of cholates can also impart handedness-based differences in the buoyancy of nanotubes.[7] Such buoyancy differences were exploited via density gradient ultracentrifugation (DGU),[4e] and further resolved via the combination of co-surfactants and nonlinear density gradients.[4b] The interdependency of chirality and handedness separation, has prevented the field thus far to sort in one step, all left- from all right-handed SWNTs, irrespective of their (*n*,*m*) chirality.

The naturally occurring flavin mononucleotide (*R*-FMN or FMN), a phosphorylated form of vitamin B_2, was recently shown to wrap around SWNTs (Figure 1a–c) and impart

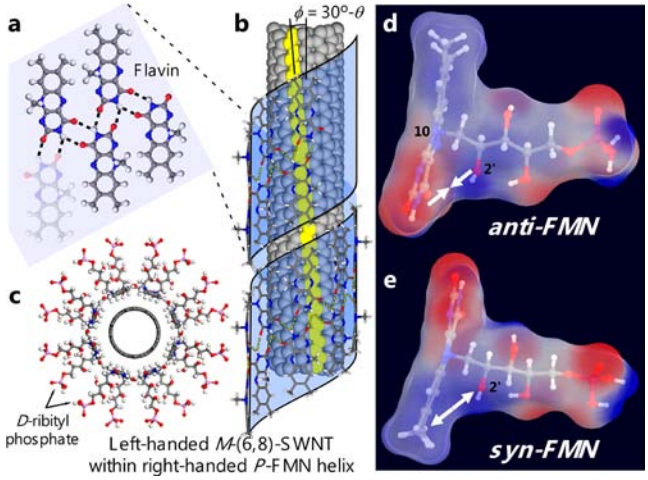

Figure 1. Adjacent H-bonds stabilize the flavin helical ribbon (a) that wraps around SWNTs (b) with the D-ribityl phosphate side groups providing aqueous solubilization (c). The sp^3 hybridization of the N(10) atom of isoalloxazine produces two conformations (d,e) for the *R*-FMN. Electrostatic attractions between the adjacent uracil and 2′-OH groups stabilize the anticonformer that leads to a right-handed FMN helix.

effective nanotube suspension with diameter distribution spanning from 0.76 to 1.17 nm, alongside (8,6)-SWNT enrichment.[5] This is a direct result of the self-organization of isoalloxazine moieties into a 2D ribbon (Figure 1b) that subsequently wraps around SWNTs with the help of concentric $\pi-\pi$ interactions, extending the D-ribityl phosphate side chains outward to facilitate aqueous dispersion. Ideally, four isomers are expected for each chiral-SWNT/flavin species (i.e., *P*/*P*, *P*/*M*, *M*/*P*, and *M*/*M*), with Figure 1c illustrating the *M*/*P* isomer. The structural similarity of FMN with nucleic acids has

Received: May 30, 2012
Published: August 7, 2012

   dx.doi.org/10.1021/ja305250g | *J. Am. Chem. Soc.* 2012, 134, 13196–13199

prompted us to investigate possible handedness selection of FMN-dispersed nanotubes. Here, we show that the helical wrapping of FMN forms a right-handed helix that naturally selects all left-handed (*n*,*m*)-SWNT species.

HiPco SWNTs were dispersed in a FMN/D_2O solution using 4 h sonication (300 W) and subjected to a 2 h centrifugation (15000*g*) to produce an optically clear, greenish-black, nanotube dispersion, as previously reported.[5] Figure S1a,b in the Supporting Information (SI) illustrates the well-individualized vis−NIR absorption and 2D photoluminescence excitation (PLE) spectra of D_2O FMN/SWNT dispersion, respectively.[8] The circular dichroism (CD) and corresponding UV−vis−NIR absorption spectra of both the D_2O/FMN solution (red-curve) and the D_2O/FMN/SWNT suspension (black curve) are shown in Figure 2a,b, respectively. The

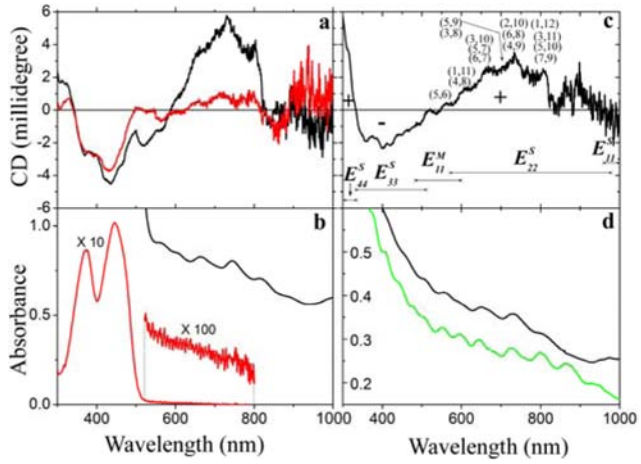

Figure 2. CD (a) and corresponding UV−vis−NIR spectra (b) of D_2O solutions of FMN (red curve) and FMN-suspended HiPco SWNTs (black curve). CD (c) and UV−vis−NIR spectra (d) following FMN replacement with SDBS (black curve). SDBS-dispersed HiPco SWNTs were used as control (green curve).

spectrum below 544 nm is overwhelmed by the FMN absorption as shown in Figure 2b. In that region, FMN exhibits a well-defined CD structure that extends at a smaller magnitude above 544 nm. The weak FMN CD spectrum above 544 nm is believed to originate from the presence of small aggregates, in accordance with the 100 times expansion of its absorption spectra in that region. On the other hand, FMN-dispersed SWNTs show a well-defined CD signal in the area of 588 and 828 nm, along with profound divergence from the FMN CD spectrum in the 300−336, 499−580, and 828−1000 nm regions.

Deciphering the true contributions of SWNTs to the CD spectra necessitates replacement of the chiral and optically absorbing FMN moiety with the achiral and optically transparent sodium dodecyl benzenesulfonate (SDBS).[9] This was accomplished with repetitive dialysis of FMN/SWNT suspension with 1% of SDBS solution in D_2O, as previously reported.[5] The complete SDBS replacement of the FMN moiety was confirmed by the lack of FMN PL as well as by the expected blue shift in the UV−vis−NIR absorptions of all observed (*n*,*m*) SWNTs (see Table S1, SI).[5] On the basis of the UV−vis−NIR and PLE maps in Figure S2a,b of the SI, the aqueous SDBS-replaced SWNTs appears to be equally dispersed as the respective mother FMN/SWNT dispersion (Figure S1a,b)). Figure 2c,d illustrates the CD and UV−vis−NIR of FMN-extracted and SDBS-replaced nanotube suspension. As expected, the elimination of FMN absorption in the 300−544 nm region, enables the observation of the underlying E^S_{44} and E^S_{33} HiPco nanotube transitions, whose regions are marked for convenience on the bottom abscissa of Figure 2c. The well-defined alternative pattern of (+,−,+) signs for the E^S_{44}, E^S_{33}, and E^S_{22} transitions, respectively, indicates that all FMN-dispersed SWNTs are left-handed enriched,[9] and SDBS does not contribute to the CD signal (Figure S3).

The handedness enantioselectivity afforded by the FMN helix begs the question on how such separation is made possible. As shown in Figure 1d,e, a salient aspect of such handedness separation originates from the fact that the N atom at the 10 position (N(10)) of the isoalloxazine ring adopts an sp^3 hybridization that can allow the adjacent rings in the helix to closely pack with themselves.[10,11] Such hybridization produces two different conformations for the D-ribityl chain, directing this chiral moiety in either sides of the isoalloxazine ring. These two conformations resemble the *syn* and *anti* conformations between glycoside and purine/pyrimidine bases of DNA. The *syn* and *anti* conformations are responsible for the formation of left-handed (i.e., Z-form) and right-handed (i.e., A- and B-form) DNA, respectively.[12] Figure 1d,e depicts the two energy-minimized conformations of FMN at the DFT/B3LYP/6-31g+(d,p) level of theory, with the hybridization of the N(10) atom fixed as sp^3 (see Methods in SI). This causes the D-ribityl phosphate side chain to reside in either side of the isoalloxazine ring, which in turn directs the polar uracil moiety closer to (*anti*) or farther from (*syn*) the 2′-hydroxyl group. The computed energy difference between the two conformers is 3.0 (1.5) kcal/mol in vacuum (water), in favor of the *anti* conformer. Such energy difference stems mainly from electrostatic interactions between the 2′-hydroxyl's dipole and the oppositely oriented dipoles of the uracil's C═N and C═O groups. The mapping of the DFT-derived electrostatic potential into the molecular surface shows that the *anti* conformer is electrostatically favored (i.e., complementary blue/red charge coloration denotes attractive interactions) as opposed to the repulsive interactions in the *syn* conformer. Since electrostatic interactions are inversely proportional to distance, the hydroxyl groups further up in the D-ribityl side chain contribute much less to the difference in energy. In accordance with DNA, the *anti*-like conformation of FMN prefers to organize in right-handed helices, as shown in Figure 1c. This is directly supported by HRTEM images published elsewhere,[5] where only right-handed helices have been observed.

The next question pertains on why the right-handed helix selects left-handed nanotubes? The two leading models invoke structural rearrangement of the FMN helix alone or some sort of "cooperative interaction" between the nanotube/FMN helices. To address the first model, we investigated the orientation tendency of the isoalloxazine rings with respect to its underlying chiral lattice, within the tight confines of the 8_1 helix. For this, we used molecular mechanics (MM) force-field calculations on the two handedness isomers of (8,6)-SWNT (i.e., *P*-(8,6) and *M*-(6,8)), since our originally predicted structure of the 8_1 helix[5] showed good agreement with that from a more advanced DFT calculation.[11] This allowed us to incorporate periodic boundary conditions for both FMN and nanotube helices by slightly contracting (ca. 5%) the 2.63 nm (8,6)-SWNT unit cell[13] to match the 2.5 nm helix period.[5]

Figure 3a,b illustrates a close-up of the starting and the energy-minimized FMN configuration (two out of the eight Σ_n

dx.doi.org/10.1021/ja305250g | J. Am. Chem. Soc. 2012, 134, 13196−13199

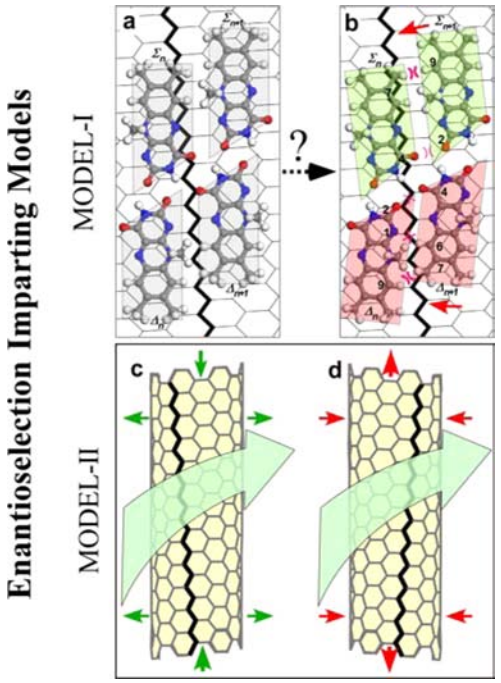

Figure 3. Two plausible models on the nature of nanotube enantioselection. Model-I: Molecular simulations on FMN rotation on rigid *M*-(6,8)- or *P*-(8,6)-SWNTs (Figure S4) indicate that the starting, "armchair-like" orientation of the isoalloxazine moieties (a) causes the Σ_n and Δ_n sub-helices to rotate opposite to each other (b). This casts doubts on the validity of this model for imparting SWNT enantioselection since the energy gains from the green-shaded Σ_n sub-helix (with optimum lattice registry) are nullified by the red-shaded Δ_n sub-helix. Model-II: The right-handed FMN helix (green arrow) exerts torsion to the nanotube similar to "Indian burn" that in the case of left-handed chiral SWNTs causes axial compression and diameter dilation (c) as opposed to right-handed nanotubes that creates axial elongation and diameter contraction (d). Here, (c) is preferred over (d) since diameter dilation enhances the intermolecular interactions between FMN helix and SWNT.

and Δ_n isoalloxazine repeats) of the right-handed FMN helix around a rigid *M*-(6,8)-SWNT (*P*-(8,6)-nanotube is shown in Figure S4). Here it is important to stress that the atomic coordinates for both *M*-(6,8) and *P*-(8,6)-SWNTs were held constant and were not allowed to relax, while the *P*-FMN helix was left free to optimize itself with respect to the underlying graphene pattern. The nanotube handedness is illustrated by the "polyacetylene chain" shown in thicker tone, while the overlaid trapezoid indicates an idealized footprint of the isoalloxazine ring. For the sake of clarity, the nanotubes in Figure 3,b are depicted in a flattened projection (i.e., hexagons stretched laterally), while Figures S5 and S6 show the longitudinal and axial projections, respectively, to illustrate the full helical pattern along with dimethyl group interdigitation developed via energy minimization. The starting *P*-FMN helix has the isoalloxazine rings oriented parallel with the longitudinal nanotube axis. Upon energy minimization, all eight Σ_n subunits rotate clockwise so that they orient along the nanotube lattice registry. Having said this, the strong H-bonding that holds the FMN ribbon together (Figure 1b) acts as a pivotal point and causes the remaining Δ_n subunits to rotate in the opposite direction. Consequently, while the Σ_n subunits improve their $\pi-\pi$ stacking interactions (green shading) the Δ_n moieties end up with a poorer alignment. No matter how carefully we attempted to align both Σ_n and Δ_n moieties along the polyacetylene chain, the lateral close packing of the helix along with the specific H-bonding pattern eventually forced them to rotate opposite to each other.

A direct consequence of such opposite rotation is the development of a number of close contacts shown in Figure 3b and analyzed in Table S2. The two prominent close contacts (2.4−2.6 Å) are between the two hydrogen atoms at the C_9 position for the Δ_n units, and the two hydrogens of the methyl group at the 7 position for the Σ_n units. Two other close contacts of lesser severity are that for N_1 to H−C_6 (2.6−2.7 Å) and for C_2═O to O═C_4 (2.8−2.9 Å). Here it is important to note that while the methyl group at the N_{10} position appears to be in close proximity to the nearest isoalloxazine ring, the N_{10} sp^3 configuration permits this methyl group to lie above the aromatic ring plane and thus renders it nonrelevant in terms of close contacts. Tables S3 and S4 along with Figures S5 and S6 illustrate the breakdown in terms of energy contribution from bonds, angles, torsions, inversions, and van del Waals (vdW), electrostatic, and H-bonding interactions for both *M*-(6,8) and *P*-(8,6)-SWNTs wrapped with *P*-FMN helix. As it turns out, the right *P*-FMN helix produces a slightly more stable assembly around a *M*-(6,8)-SWNTs (by 1.2 kcal/mol or 52 meV) as compared to *P*-(8,6)-SWNTs. Taking into consideration the fact that the average H-bonding energy is comparable for Σ_n/Δ_n and Σ_n/Δ_{n+1} pairs for both complexes (Figure S7), it is safe to conclude that half of stabilization (0.6 kcal/mol) can be ascribed from improved vdW between FMN helix and nanotube, while the other half is attributed to internal (bonded and nonbonded) stabilization within the FMN helix on the *M*-(6,8)-SWNT (Table S3). This puts in question whether such small energy difference (ca. $2k_BT$) can explain enantioselection for such a large assembly, hence the question mark above the dotted arrow in Figure 3. Moreover, since the FMN rotation of Model-I is limited to small angles of ϕ (ca. 5−6° before close contacts render it prohibitive), it becomes apparent that structural rearrangement of FMN alone cannot fully address the experimental results of Figure 2, where enantioselection for nanotubes with much larger ϕ or smaller chiral angles θ ($\phi \approx 30° - \theta$) occurs.

With this in mind, we redirect our focus to the second model (Model-II) where enantioselectivity originates from a "cooperative interaction" between the nanotube and its FMN helix. One possibility is that the right-handed FMN helix due to its close-packed nature, imposes a right twist to the nanotube resembling "Indian burn". Recent reports show that small nanotube twists are not that energetically expensive, and can certainly be accommodated within k_BT.[14,15] Such a twist, could (in principle) improve intermolecular interactions of both Σ_n and Δ_n moieties with the underlying graphene lattice. Using classical molecular dynamics based on second-generation reactive empirical bond order (REBO) potentials that sufficiently describe C−C interactions in graphite and diamond, Upmanyu et al.[16] has shown that all (*n*,*m*) chiral nanotubes exhibit asymmetric torsional response to an externally applied strain. What is more important, however, is that twisting chiral nanotubes toward the armchair configuration causes them to compress axially and dilate radially (Figure 3c). On the other hand, a twist in the opposite direction (toward the zigzag configuration) causes them to expand axially and shrink diametrically (Figure 3d). This indicates that when a right-handed twist is applied to all left-handed *M*-(*m*,*n*) nanotubes,

Table 1. Resonance Raman RBM and ω_{G+} Shifts of Sodium Cholate (SC) and FMN (with Low Coverage (*lc*) and High Coverage (*hc*)) Dispersed SWNTs of Varying Chiral Angle θ

			ω_{RBM} (cm^{-1})			$\Delta\omega_{RBM}$ (cm^{-1})		ω_{G+} (cm^{-1})			$\Delta\omega_{G+}$ (cm^{-1})	
(*n*,*m*)	θ (°)	E_{laser}(eV)	SC	FMN,*lc*	FMN,*hc*	*hc* − *lc*	SC − *hc*	SC	FMN,*lc*	FMN,*hc*	*hc* − *lc*	SC − *hc*
(7,5)	24.5	1.96	283.4	286.8	287.8	1.0	4.4	1594.5	1595.4	1593.6	−1.8	−0.9
(10,2)	8.9	1.58	265.8	266.4	267.7	1.3	1.9	1592.9	1592.8	1591.0	−1.8	−1.9

these should exhibit improved intermolecular interactions between nanotube and FMN helix due to diameter dilation.

To ascertain whether the FMN helix induces SWNT torsion, we resorted to resonance Raman spectroscopy (RRS). Knowing that increasing amount of FMN improves nanotube coverage and helix perfection,[5] we performed RRS on SWNTs with low and high FMN coverage (*lc* and *hc*, respectively; see Methods in SI and Figures S8 and S9). It is well known that nanotube twist incurs a frequency downshift on the longitudinal G-band.[17] This trend is observed with increasing coverage, as shown by the $\Delta\omega_{G+}$ (*hc* − *lc*) column in Table 1, despite an otherwise expected upshift due to FMN-induced nanotube *p*-doping.[11] In terms of radial breathing mode (RBM), nanotube torsion has been reported to upshift ω_{RBM}.[17a] This is witnessed with all resolvable (*n*,*m*) nanotubes in Table 1 (Figure S9), using the two laser lines that are above 600 nm to avoid FMN fluorescence. Here, the FMN-induced charge transfer[5] provides an initial stiffening of the FMN/SWNT complex, causing an appreciable upshift with respect to the ω_{RBM} of sodium cholate (SC)-dispersed SWNTs. By increasing FMN coverage, an additional upshift is witnessed ($\Delta\omega_{RBM}$ (*hc* − *lc*) column). Furthermore, the increasing magnitude in $\Delta\omega_{RBM}$ shift for nanotubes with increasing chiral angle (θ) provides an additional indication in support of FMN-induced nanotube twist ($\Delta\omega_{RBM}$ (SC − *hc*) column).[17c] These RRS findings provide strong initial support that the observed enantioselection is linked with FMN-induced nanotube twisting (Model II). Having said this, more refined molecular simulations together with tunable excitation RRS studies are needed in order to resolve more (*n*,*m*)-SWNTs and fully quantify the interplay between nanotube twist and FMN-induced torsion, to be investigated in future publications. These studies can ultimately decipher whether nanotube twisting is the cause of the unique, FMN-induced, family- and modality-dependent red-shift pattern, observed in ref 5, as well as DGU-based SWNT enantioselection,[4b] via handedness-specific diameter variations.

■ ASSOCIATED CONTENT

Supporting Information

Methods, UV−vis−NIR, PLE maps, RRS, and molecular mechanics analysis. This material is available free of charge via the Internet at http://pubs.acs.org.

■ AUTHOR INFORMATION

Corresponding Author

papadim@mail.ims.uconn.edu

Present Address

[§]Department of Chemistry, Yonsei University, Seoul, Korea

Author Contributions

[⊥]S.-Y.J. and D.C.A. contributed equally.

Notes

The authors declare no competing financial interest.

■ ACKNOWLEDGMENTS

Financial support by AFOSR FA9550-09-1-0201, and in part by NSF IIP-0930494 and CBET-0828771/0828824 and NIH ES013557, is kindly acknowledged.

■ REFERENCES

(1) (a) Cram, D. J. *Science* **1988**, *240*, 760. (b) Maier, N. M.; Franco, P.; Lindner, W. *J. Chromatogr. A* **2001**, *906*, 3.

(2) Wildöer, J. W. G.; Venema, L. C.; Rinzler, A. G.; Smalley, R. E.; Dekker, C. *Nature* **1998**, *391*, 59.

(3) (a) Peng, X.; Komatsu, N.; Bhattacharya, S.; Shimawaki, T.; Aonuma, S.; Kimura, T.; Osuka, A. *Nat. Nanotechnol.* **2007**, *2*, 361. (b) Strano, M. S. *Nat. Nanotechnol.* **2007**, *2*, 340.

(4) (a) Tu, X.; Manohar, S.; Jagota, A.; Zheng, M. *Nature* **2009**, *460*, 250. (b) Ghosh, S.; Bachilo, S. M.; Weisman, R. B. *Nat. Nanotechnol.* **2010**, *5*, 443. (c) Liu, H.; Nishide, D.; Tanaka, T.; Kataura, H. *Nat. Commun.* **2011**, *2*, 309. (d) Nish, A.; Hwang, J. Y.; Doig, J.; Nicholas, R. J. *Nat. Nanotechnol.* **2007**, *2*, 640. (e) Arnold, M. S.; Green, A. A.; Hulvat, J. F.; Stupp, S. I.; Hersam, M. C. *Nat. Nanotechnol.* **2006**, *1*, 60.

(5) Ju, S. Y.; Doll, J.; Sharma, I.; Papadimitrakopoulos, F. *Nat. Nanotechnol.* **2008**, *3*, 356.

(6) (a) Peng, X.; Komatsu, N.; Kimura, T.; Osuka, A. *J. Am. Chem. Soc.* **2007**, *129*, 15947. (b) Peng, X.; Komatsu, N.; Kimura, T.; Osuka, A. *ACS Nano* **2008**, *2*, 2045. (c) Wang, F.; Matsuda, K.; Rahman, A. F. M. M.; Peng, X.; Kimura, T.; Komatsu, N. *J. Am. Chem. Soc.* **2010**, *132*, 10876.

(7) Green, A. A.; Duch, M. C.; Hersam, M. C. *Nano Res.* **2009**, *2*, 69.

(8) Bachilo, S. M.; Strano, M. S.; Kittrell, C.; Hauge, R. H.; Smalley, R. E.; Weisman, R. B. *Science* **2002**, *298*, 2361.

(9) Dukovic, G.; Balaz, M.; Doak, P.; Berova, N. D.; Zheng, M.; McLean, R. S.; Brus, L. E. *J. Am. Chem. Soc.* **2006**, *128*, 9004.

(10) (a) Kierkegaard, P.; Norrestam, R.; Werner, P.-E.; Csöregh, I.; von Glehn, M.; Karlsson, R.; Leijonmark, M.; Rönnquist, O.; Stensland, B.; Tillberg, O.; Torbjörnssen, L. In *Flavins and Flavoproteins, Third International Symposium*; Kamin, H., Ed.; University Park Press: Baltimore, 1971; pp 1−22. (b) Beinert, W.-D.; Ruterjans, H.; Muller, F. *Eur. J. Biochem.* **1985**, *152*, 573.

(11) Ogunro, O. O.; Wang, X. Q. *Nano Lett.* **2009**, *9*, 1034.

(12) (a) Blackburn, G. M.; Gait, M. J. *Nucleic Acid and Chemistry and Biochemistry*, 2nd ed.; Oxford University Press: New York, 1996; pp 24−25. (b) Dickerson, R. E.; David, M. D. *Methods in Enzymology*; Academic Press: San Diego, CA, 1992; Vol. *211*, p 67.

(13) Dresselhaus, M. S., Dresselhaus, G., Avouris, P., Eds. *Carbon nanotubes: Synthesis, Structure, Properties and Applications*; Springer: Berlin, 2001.

(14) (a) Kwon, Y. K.; Tománek, D. *Phys. Rev. Lett.* **2000**, *84*, 1483. (b) Wang, S.; Wang, R.; Wu, X.; Zhang, H.; Liu, R. *Phys. E Low Dimens. Syst. Nanostruct.* **2010**, *42*, 2250.

(15) Liu, Z.; Qin, L. C. *Carbon* **2005**, *43*, 2146.

(16) Liang, H.; Upmanyu, M. *Phys. Rev. Lett.* **2006**, *96*, 165501.

(17) (a) Gao, B.; Duan, X.; Zhang, J.; Wu, T.; Son, H.; Kong, J.; Liu, Z. *Nano Lett.* **2007**, *7*, 750. (b) Li, X.; Jia, Y.; Dong, J.; Kawazoe, Y. *Phys. Rev. B* **2010**, *81*, 195439. (c) Yang, L.; Han, J. *Phys. Rev. Lett.* **2000**, *85*, 154.